Results in Physics 7 (2017) 2361–2368

Contents lists available at ScienceDirect

Results in Physics

journal homepage: www.journals.elsevier.com/results-in-physics

Mathematical analysis of ferromagnetic fluid embedded in a porous medium

Sohail Nadeem [a], Irum Raishad [a,*], Noor Muhammad [a], M.T. Mustafa [b]

[a] Department of Mathematics, Quaid-I-Azam University 45320, Islamabad 44000, Pakistan
[b] Department of Mathematics, Statistics and Physics, College of Arts and Science Qatar University, Qatar

ARTICLE INFO

Article history:
Received 6 May 2017
Received in revised form 29 May 2017
Accepted 9 June 2017
Available online 9 July 2017

Keywords:
Ferrofluid
Thermal stratification
Magnetic dipole
Stagnation point flow

ABSTRACT

This article focuses on the impacts of heat transport phenomenon in a ferrofluid in presence of a magnetic dipole. The flow is caused by stretching of the surface. The analysis is disclosed with porous medium and thermal stratification. The characteristics of thermomechanical coupling are computed analytically and numerically. It is depicted that the porous medium has the significant effect in controlling the rate of heat transfer in the boundary layer. Drag coefficient at the surface reduces when larger ratio parameter is considered. Comparison of present study with previous published work is given. The results are found in excellent agreement.

Introduction

Stephen [1] invented the ferrofluid in 1965. These fluids are magnetic fluids with low viscosity, which are prepared through the colloidal suspension of magnetic particles. The presence of magnetic field makes ferrofluid strongly magnetized. Ferrofluids can be used to image magnetic domain structures on the surface of ferromagnetic materials using a technique developed by Francis Bitter [2]. Ferromagnetic fluids have obvious significance in modern technology and industry. These fluids provided basis for some chemical and electromechanical devices, for instance, transformers, rotating X-ray tubes, electric engines, electromagnets, generators, and hoarding (e.g. hard plates and recording procedures), while in biological sciences, we can use in magnet therapy for pain management, gout, cure arthritis, spondicitis, migraines and headaches, and magnetic resonance imaging etc. Anderson and Valnes [3] initiated ferromagnetic fluid flow induced by stretching sheet and explored the effects of magneto-thermomechanical on boundary layer flow. The characteristics of thermal and magnetic field gradients were studied by Neuringer et al. [4] in a saturated ferrofluid flow. Tzirtzilakis et al. [5] analyzed sundry materialized parameters numerically to study the impact of a localized magnetic field over a forced and free convective magnetic fluid flow. Sharma et al. [6] identified the characteristics of dust particles on a ferromagnetic fluid in a porous medium with thermal convection. Heat transfer analysis in a ferrofuid flow over a stretching surface in presence of magnetic dipole are exposed by Majeed et al. [7]. The influence of dust particles with thermal convection in a ferromagnetic fluid is observed by Sharma et al. [8]. Furthermore, ferrofluid has a notable fascinating characteristic that is magnetization is a function of temperature, so ferrofluids are more competent in diverse practical applications due to this thermomagnetic coupling, see [9,10]. Albrecht et al. [11] originated domains for the ferromagnetism and ferromagnetic effects in a liquid metal.

Viscous fluid with the characteristics of thermal stratification has got extensive significance among the scientists. Thermal stratification along viscous liquids are applicable in many industrial and engineering processes. It starts in fluid flows due to changes in their temperature difference, or different densities of liquids. Srinivasacharya and Upendar [12]exposed the impact of double stratification on magnetohydrodynamic free convection in a micropolar fluid. In addition, magnetohydrodynamic fluid flow with high porosity medium and thermal stratification over an inclined plate are scrutinized by Foisal and Alam [13]. Superposed porosity with thermal stratification and shear flows in pure fluid domains is solved through numerical technique by Antoniadis and Papalexandris [14]. Ganesh et al. [15] examined the second order slip, viscous effects and Ohmic dissipations in a thermally stratified porous medium of a hydrodynamic nanofluid over a shrinking/stretching sheet. Ferdows and Liu [16] illustrates the characteristics of inertia with internal heat generation on free convection from a horizontal sheet surrounded in a porous medium.

* Corresponding author.
E-mail address: irumraishad@gmail.com (I. Raishad).

http://dx.doi.org/10.1016/j.rinp.2017.06.007
2211-3797/

It is well-known fact that the evaluation of stretchable surfaces surrounded by fluids leads to extensive features of industrial and technological significance including glass blowing, paper production, crystal growing, and aerodynamics extrusion of plastic materials etc. As the impacts of partial slip and magnetohydrodynamics are observed by Nadeem et al. [17] on obliquely striking rheological fluid past a stretching surface. Rashidi et al. [18] explored heat transfer in a transverse magnetic fluid flow saturated in a porous medium. Further, the impact of magnetic field over a stretching surface in a suspension of nanoparticles and gyrotactic microorganisms is scrutinized by Akbar and Khan [19]. Nadeem and Muhammad [20] proposed the influence of theory of the Cattaneo-Christov and stratification in the flow over a stretching sheet. Nadeem et al. [21] inspected convective heat transfer in slip flow over a stretching surface in the presence of carbon nanotubes along with the impact of magnetohydrodynamics. Some applications may be found in [22–35].

To the best of our knowledge, no one has depicted the impacts of thermal stratification and stagnation point in a ferromagnetic Jeffrey fluid saturated with a porous medium over a linear stretching sheet. We are interested here in explaining the characteristics of stagnation point and thermal stratification in a Jeffrey fluid in presence of magnetic dipole. The medium is taken to be porous. The respective equations are considered under the assumptions of a boundary layer. After utilizing the similarity variables the resulting differential equations are solved numerically and analytically with the help of BVPh2–midpoint method and OHAM respectively. Physical features are interpreted through graphs and tables.

Ferrohydrodynamic and thermal energy equations

Flow analysis

An electrically non-conducting, steady and an incompressible two- dimensional ferrofluid is merged over a linear stretching sheet. The stretching is initiated in the sheet having velocity $U_w(x)$ due to a force exerted on the sheet at $y = 0$. The stretching is directly proportional to the distance from the origin. The magnetic dipole is arranged on outer surface at some distance from the fluid. A magnetic dipole is precisely put in the system in such a manner that its center lies at a distance b from the x-axis on the y-axis. The direction of the magnetic field lines due to magnetic dipole are in the positive x-direction. A notable strength of magnetic field is shown by the saturating ferrofluid. Curie temperature T_c is greater than the temperature at stretching sheet T_w is taken, whereas temperature of the fluid element away from the sheet is considered $T = T_\infty$ and $T_c > T_\infty > T_w$. The magnetic effect vanishes beyond the temperature T_c. Variable temperature $T_w = T_0 + c_1x, T_\infty = T_0 + c_2x$ are scrutinized at the sheet distant from the surface. The influence of heat generation is imperceptibly small. For ferrofluid, the governing boundary layer equations and heat transferring rate are shown as

$$\frac{\partial u}{\partial x}+\frac{\partial v}{\partial y}=0, \tag{1}$$

$$u\frac{\partial u}{\partial x}+v\frac{\partial u}{\partial y}=\frac{\upsilon}{1+\lambda_2}\left[\frac{\partial^2 u}{\partial y^2}+\lambda_1\left(u\frac{\partial^3 u}{\partial x\partial y^2}+v\frac{\partial^3 u}{\partial y^3}-\frac{\partial u}{\partial x}\frac{\partial^2 u}{\partial y^2}+\frac{\partial u}{\partial y}\frac{\partial^2 u}{\partial x\partial y}\right)\right] +\mu_0 M\frac{\partial H}{\partial x}-\frac{\upsilon\epsilon u}{K_2}, \tag{2}$$

$$\rho C_p\left(u\frac{\partial T}{\partial x}+v\frac{\partial T}{\partial y}\right)+\mu_0 T\frac{\partial M}{\partial T}\left(u\frac{\partial H}{\partial x}+v\frac{\partial H}{\partial y}\right)=K\frac{\partial^2 T}{\partial y^2}. \tag{3}$$

Here u, v are the velocity components along x- and y-directions respectively, α exemplify thermal diffusibility, ρ displays for fluid density, υ signify the kinematic viscosity of fluid, p indicate pressure, c_p represents the specific heat, whereas α exemplify thermal diffusibility, μ_0 signify the magnetic permeability, T symbolize the temperature, H represents the magnetic field, M denotes the magnetization.

The pertinent boundary conditions are of the form

$$u|_{y=0}=U_w(x)=a_1x,\quad v|_{y=0}=0,\quad T|_{y=0}=T_w=T_0+c_1x,$$
$$u|_{y\to\infty}\to U_e(x)=a_2x,\quad T|_{y\to\infty}\to T_\infty=T_0+c_2x. \tag{4}$$

In above equations, $U_w(x)$ indicates the stretching velocity, a_1 and a_2 are dimensionless constants, T_0 identify reference temperature, whereas T_∞ define the temperature of an ambient fluid, c_1 and c_2 are the dimensional constants.

Magnetic dipole

The magnetic dipole produces the magnetic field that influences the ferrofluid flow, which is described by a magnetic scalar potential $\Omega^\star$ as

$$\Omega^{\star}=\frac{\alpha_1}{2\pi}\frac{x}{x^2+(y+b)^2}, \tag{5}$$

here α_1 illustrate the magnetic field strength at the source. The components of the magnetic field H are given by

$$\frac{\partial H}{\partial x}=-\frac{\partial\Omega^{\star}}{\partial x}=\frac{\alpha_1}{2\pi}\frac{x^2-(y+b)^2}{\left((y+b)^2+x^2\right)^2}, \tag{6}$$

$$\frac{\partial H}{\partial y}=-\frac{\partial\Omega^{\star}}{\partial y}=\frac{\alpha_1}{2\pi}\frac{2x(y+b)}{\left((y+b)^2+x^2\right)^2}, \tag{7}$$

since the magnetic body force is (generally) proportional to the gradient of the magnetic of H, in this manner we have

$$H=\sqrt{\left(\frac{\partial\Omega^{\star}}{\partial x}\right)^2+\left(\frac{\partial\Omega^{\star}}{\partial y}\right)^2}. \tag{8}$$

Making use of Eqs. (6) and (7) in Eq. (8), we get the successive equations, after expanded in powers of x and held terms up to order x^2 ,

$$\frac{\partial H}{\partial x}=-\frac{\alpha_1}{2\pi}\frac{2x}{(y+b)^4}, \tag{9}$$

$$\frac{\partial H}{\partial y}=\frac{\alpha_1}{2\pi}\left(\frac{4x^2}{(y+b)^5}-\frac{2}{(y+b)^3}\right). \tag{10}$$

Effect of magnetization M with temperature T is given by the linear expression below,

$$M=K^*(T-T_\infty), \tag{11}$$

here K^* denotes the pyromagnetic co-efficient. The physical schematic of a heated ferrofluid appears in Fig. 1. Here the roundabout lines demonstrate the magnetic field.

Solution procedure

Here we compose the dimensionless variables as perceived by Anderson [9]

$$\psi(\zeta,\xi)=\zeta\left(\frac{\mu}{\rho}\right)f(\xi),$$
$$\theta(\zeta,\xi)\equiv\frac{T_\infty-T}{T_0-T_w}=\theta_1(\xi)+\zeta^2\theta_2(\xi), \tag{12}$$

here $\theta_1(\zeta,\xi)$ and $\theta_2(\zeta,\xi)$ exhibits dimensionless temperature and μ express dynamic viscosity, the corresponding non-dimensional coordinates are

$$\zeta=\left(\frac{\rho a_1}{\mu}\right)^{1/2}x,\quad \xi=\left(\frac{\rho a_1}{\mu}\right)^{1/2}y. \tag{13}$$

The stream function is defined in such a way that the continuity equation is directly satisfied, here the stream function $\psi(\zeta,\xi)$ and the comparable velocity components u and v are defined as

$$u=\frac{\partial\psi}{\partial y}=xa_1f'(\xi),\quad v=-\frac{\partial\psi}{\partial x}=-(\upsilon a_1)^{1/2}f(\xi), \tag{14}$$

where prime expresses differentiation with respect to ξ. Applying the boundary layer approximation $(O(x)=O(u)=O(1)$ and $O(y)=O(v)=O(\delta))$ and using similarity variables given in Eqs. (12)–(14), the Eqs. (2) and (3) along with boundary conditions given in Eq. (4) reduces to the following system of equations and corresponding boundary conditions

$$f'''-(1+\lambda_2)(f'^2-ff'')+\gamma_1(f''^2-ff^4)-(1+\lambda_2)\frac{2\beta\theta_1}{(\xi+\alpha_1)^4}+P_m(R^2-f')=0, \tag{15}$$

$$\theta_1''+\mathrm{Pr}f\theta_1'+\frac{2(\theta_1-\varepsilon)\lambda\beta f}{(\xi+\alpha_1)^3}+2\theta_2-4f'^2\lambda=0, \tag{16}$$

$$\theta_2''+\mathrm{Pr}(f\theta_2'-2f'\theta_2)+\frac{2\lambda\beta f\theta_2}{(\xi+\alpha_1)^3}-\lambda\beta(\theta_1-\varepsilon)\left(\frac{2f'}{(\xi+\alpha_1)^4}+\frac{4f}{(\xi+\alpha_1)^5}\right)-4\lambda f''^2=0, \tag{17}$$

$$f(\xi)=0,f'(\xi)=1,\theta_1(\xi)=1-S_1,\theta_2(\xi)=0,\quad \text{at } \xi=0, \tag{18}$$

$$f'(\xi)\to R,\theta_1(\xi)\to 0,\theta_2(\xi)\to 0,\quad \text{when } \xi\to\infty. \tag{19}$$

In above system of nonlinear equations, the parameters of β (ferrohydrodynamic interaction), γ_1 (Deborah number), S_1 (thermal stratified parameter), λ (viscous dissipation), R (ratio), P_m (the permeability of porous medium), ε (curie temperature) and Pr (Prandtl number) are defined as

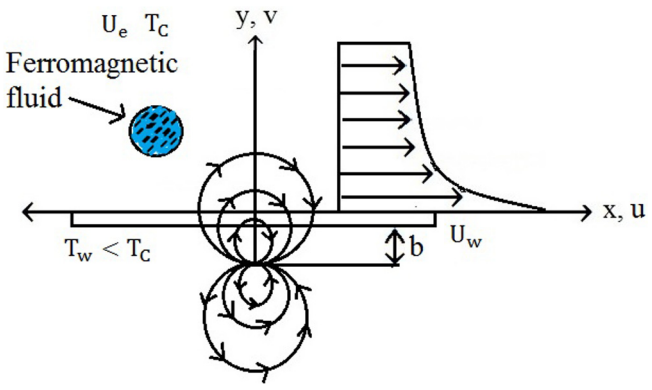

Fig. 1. Geometry of the flow.

$$\mathrm{Pr}=\frac{\upsilon}{\alpha},\quad R=\frac{a_2}{a_1},\quad \beta=\frac{\alpha_1}{2\pi}\frac{(T_0-T_w)\mu_0K\rho}{\mu^2},\quad \varepsilon=\frac{T_\infty}{T_0-T_w},\quad \gamma_1=\lambda a_1,$$
$$S1=\frac{c_2}{c_1},\quad P_m=\frac{\upsilon\epsilon}{K_2a_1},\quad \lambda=\frac{a_1\mu^2}{(T_0-T_w)\rho k},\quad \gamma=\sqrt{\frac{a_1\rho b^2}{\mu}}. \tag{20}$$

Skin friction coefficient and Nusselt number are defined as

$$C_f=\frac{-2\tau_w}{\rho U_w^2},\quad Nu=\frac{x}{T_0-T_w}\frac{\partial T}{\partial y}\Big|_{y=0},\quad \tau_w=\mu\frac{\partial u}{\partial y}\Big|_{y=0}. \tag{21}$$

Using the similarity variables the following dimensionless expressions are obtained

$$\mathrm{Re}^{1/2}C_f=-2f''(0),\quad \mathrm{Re}^{-1/2}Nu=-(\theta_1'(0)+\zeta^2\theta_2'(0)). \tag{22}$$

Optimal homotopy analysis method

Optimal homotopy analysis method is employed for a solution of the problem. The method is used to interpret the solutions for highly non-linear problems. The optimal homotopy analysis method gives us a better flexibility to get the auxiliary linear operator and the initial guess than the conventional nonperturbative techniques, as pointed out later by Liao [36,37]. The linear operators and initial guesses for the existing flow problem are

$$\mathcal{L}_f(f)=\frac{d^3f}{d\xi^3}+\frac{d^2f}{d\xi^2},\quad \mathcal{L}_{\theta_1}(\theta_1)=\frac{d^2\theta_1}{d\xi^2}-\theta_1,\quad \mathcal{L}_{\theta_2}(\theta_2)=\frac{d^2\theta_2}{d\xi^2}-\theta_2, \tag{23}$$

$$f_0(\xi)=1+R(\xi-1)-(1-R)\exp(-\xi),$$
$$\theta_{1_0}(\xi)=(1-S_1)\exp(-\xi),$$
$$\theta_{2_0}(\xi)=\xi\exp(-\xi). \tag{24}$$

where $\mathcal{L}_f(f),\mathcal{L}_{\theta_1}(\theta_1)$ and $\mathcal{L}_{\theta_2}(\theta_2)$ portray the linear operators, furthermore, $f_0(\xi),\theta_{1_0}(\xi)$ and $\theta_{2_0}(\xi)$ exemplify the respective initial guesses of f_0,θ_{1_0} and θ_{2_0}.

Convergence analysis

The auxiliary parameters $\hbar_f,\hbar_{\theta_1}$ and $\hbar_{\theta_2}$ have a magnificent aim to stabilize and control the convergence of homotopic solutions. To get convergent solutions, we take preferred values of these parameters. For this purpose, residual errors are scrutinized for momentum and energy equations by implementing the equations given below

$$\Delta_m^f=\int_0^1\left[\mathcal{R}_m^f(\xi,\hbar_f)\right]^2d\xi, \tag{25}$$

$$\Delta_m^{\theta_1}=\int_0^1\left[\mathcal{R}_m^{\theta_1}(\xi,\hbar_{\theta_1})\right]^2d\xi, \tag{26}$$

$$\Delta_m^{\theta_2}=\int_0^1\left[\mathcal{R}_m^{\theta_2}(\xi,\hbar_{\theta_2})\right]^2d\xi. \tag{27}$$

The convergence of the parametric values is computed by optimal homotopy analysis method (Tables 1–4).

The graphical representation for the 10th and 12th order approximation shows the error decay in the following Figs. 2 and 3.

The total discrete squared residual error Δ_m^t are described through the following equation.

$$\Delta_m^t=\Delta_m^f+\Delta_m^{\theta_1}+\Delta_m^{\theta_2}. \tag{28}$$

Here the Δ_m^t is utilized to obtain the optimal convergence control parameters.

Table 1
Shows the average residual square errors (Δ_m^t) are tabulated.

$\frac{values\rightarrow}{order\downarrow}$	h_f	h_{θ_1}	h_{θ_2}	Δ_m^t
4	−0.981921	−0.872958	−0.09223	4.61754×10^{-8}
6	−0.01206	−0.943273	−0.02714	1.59062×10^{-11}
8	−0.05365	−0.914006	−0.06445	6.70151×10^{-15}
10	−0.04371	−0.05362	−0.01794	1.01087×10^{-18}
12	−0.03177	−0.92185	−0.06242	4.11943×10^{-22}

Table 2
Shows individual residual square errors for $\Delta_m^f, \Delta_m^\theta$ and Δ_m^ϕ.

$\frac{values\rightarrow}{order\downarrow}$	$h_f = -0.04371$	$h_{\theta_1} = -0.05362$	$h_{\theta_2} = -0.01794$
	Δ_m^f	$\Delta_m^{\theta_1}$	$\Delta_m^{\theta_2}$
4	1.10421×10^{-9}	3.42476×10^{-7}	3.63257×10^{-6}
8	3.54190×10^{-17}	2.51890×10^{-12}	4.44569×10^{-10}
12	8.43786×10^{-20}	7.42327×10^{-16}	5.65326×10^{-14}
20	2.56190×10^{-23}	0.53438×10^{-21}	7.96546×10^{-20}

Table 3
Comparison of Nusselt number for the case when $\beta = Pm = \gamma_1 = \lambda_2 = S_1 = \lambda = \varepsilon = \gamma = 0$.

Pr	Abel et al. [38]	$\frac{\text{Zeeshan and Majeed}}{-\theta_1'(0)}$ [7]	$\frac{\text{OHAM results}}{-\theta_1'(0)}$	$\frac{BVPh2-\text{Midpoint}}{-\theta_1'(0)}$
0.72	1.0885	1.088534	1.088542	1.0882302
1.0	1.3333	1.333347	1.333341	1.3332183
2.0	–	–	2.021082	2.0215192
3.0	–	2.509729	2.509783	2.5097533
4.0	–	–	2.903042	2.9034172
10.0	4.7968	4.796874	–	4.7868615

Results and discussion

Optimal homotopy analysis method is used to get the solution of the boundary value problem described in Eqs. (15)–(19). Here the effects of sundry physical parameters on the flow field are under discussion. The impacts of dimensionless parameters λ (viscous dissipation), β (ferrohydrodynamic interaction), S_1 (thermal stratified), γ (dimensionless distance from origin to center of magnetic dipole), R (ratio), and Pr (Prandtl number) are scrutinized. Moreover, other parameters in the flow framework are fixed. The fixed values of the parameters are taken as $\varepsilon = 2.0, \lambda = 0.01, \gamma = 1.0$.

Impacts of parameter β (ferrohydrodynamic interaction parameter)

In this subsection, we discuss the influence of β (ferrohydrodynamic interaction) parameter. The impact of ferromagnetic effect on flow problem is stabilized by the existence of β (ferrohydrodynamic interaction), ε (Curie temperature) and γ (dimensionless distance from origin to center of magnetic dipole) parameters. In Fig. 4 velocity field reduces by the increment in β (ferrohydrodynamic interaction) parameter because of the presence of ferrite particles which arises the viscosity of the fluid. The characteristics of parameter β (ferrohydrodynamic interaction) on temperature profile are shown in Fig. 5. It is observed that, by varying the parameter β (ferrohydrodynamic interaction), temperature of fluid inside the boundary layer increases. This occurs by the interaction between movements of fluid particles and an action of a magnetic field. The interaction between magnetic field action and fluid particles diminishes the velocity of the fluid whereas frictional heating among fluid layers is growing which leads to the thickness of the thermal boundary layer i.e., enhancement in heat transfer occurs due to the reduction in movements of fluid particles, which is evident in Fig. 5.

The influence of parameters S_1 (thermal stratification)

The present study characterizes the effect of parameter S_1 (thermal stratification) on velocity and temperature fields. Velocity and temperature field are decreasing for greater values of the corresponding parameter thermal stratification shown in Figs. 6 and 7. It is noted that the decaying temperature difference between surface and ambient of sheet is reducing the temperature field. Magnetohydrodynamic interaction parameter β is responsible for a reduction in axial velocity and heat transfer is raised by increasing parameter S_1 (thermal stratified), leads to increasing the density of fluid. As magnetohydrodynamic interaction is raised by the high density of ferrite particles moving towards the surface.

The influence of parameters γ_1 (Deborah number) and λ_2 (ratio of relaxation to retardation time)

This subsection concerns about the impacts of parameters γ_1 (Deborah number) and λ_2 (ratio of relaxation to retardation times). Fig. 8 shows the impact of Deborah number γ_1 on temperature field. Increasing the values of parameter γ_1 (Deborah number), there is a diminishing in temperature field $\theta_1(\xi)$. Physically γ_1 is corresponding to retardation time λ_1, thus, an extensive retardation time of any material makes it less viscous, which may bring about an enhancement in its movement, which subsequently debilitates the thermal boundary layer thickness and lower temperature field. Further, Fig. 9 depicts the impact of the ratio of relaxation to retardation time parameter λ_2 on temperature profile $\theta_1(\xi)$. From figure, it is watched that temperature profile is slowly expanding with an expansion in the value of λ_2. An enhancement in λ_2 infers to an enhancement in relaxation time and decline in retardation time. This adjustment in relaxation and retardation times

Table 4
The skin friction coefficient $-\mathrm{Re}^{-1/2}C_f$ and local Nusselt number $-\mathrm{Re}^{1/2}Nu_x$ for different values of β, γ_1, S_1 and Pr are tabulated via analytic solution based on optimal homotopy analysis method.

Pr	β	γ_1	S_1	$-\mathrm{Re}^{-1/2}C_f$	$-\mathrm{Re}^{1/2}Nu_x$
1.0	1.0	0.7	0.2	1.08721	1.28703
1.5				1.06532	2.08518
2.5				1.00532	2.34319
2.0	1.0	0.7	0.2	1.29365	2.44380
	1.4			1.45329	2.31437
	1.8			1.55430	2.31981
2.0	1.0	0.4	0.2	1.54828	0.95285
		0.8		1.32063	0.97275
		1.2		1.15042	0.98421
2.0	1.0	0.2	0.2	1.15476	0.79654
			0.4	1.16543	0.87542
			0.6	1.18043	0.96432

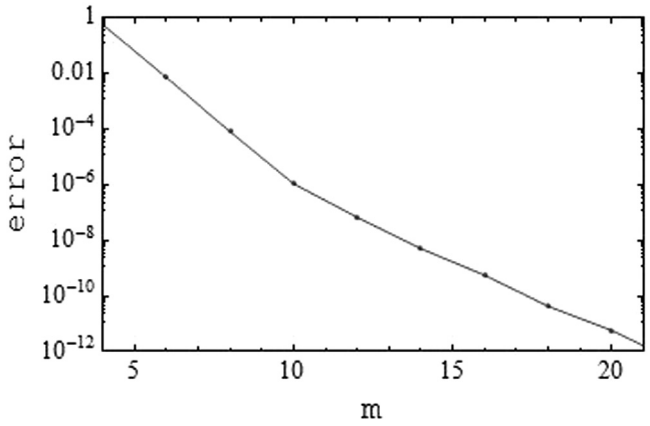

Fig. 2. The error decay for the 10th order approximation.

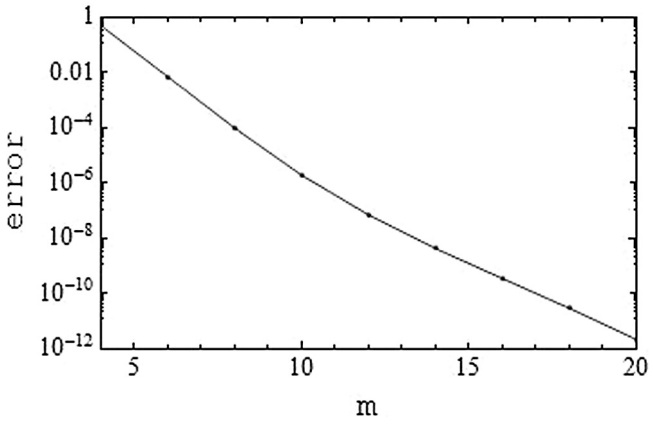

Fig. 3. The error decay for the 12th order approximation.

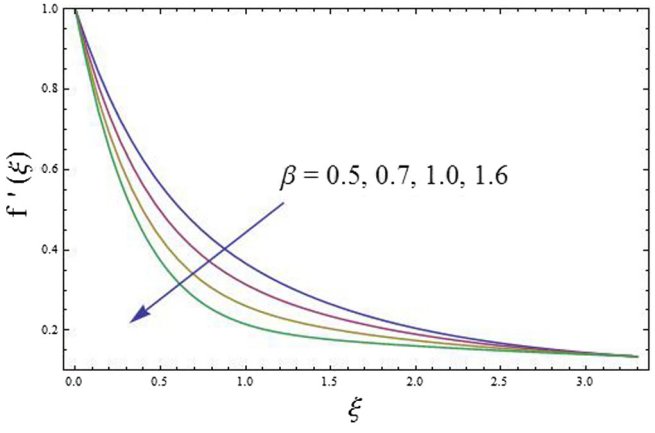

Fig. 4. Impact of ferrohydrodynamic interaction parameter 3*b*2 on velocity profile $f'(\xi)$.

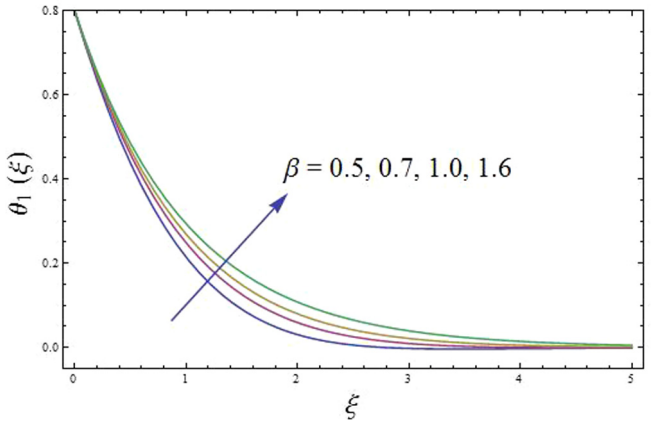

Fig. 5. Influence of ferrohydrodynamic interaction parameter 3*b*2 on temperature field $\theta_1(\xi)$.

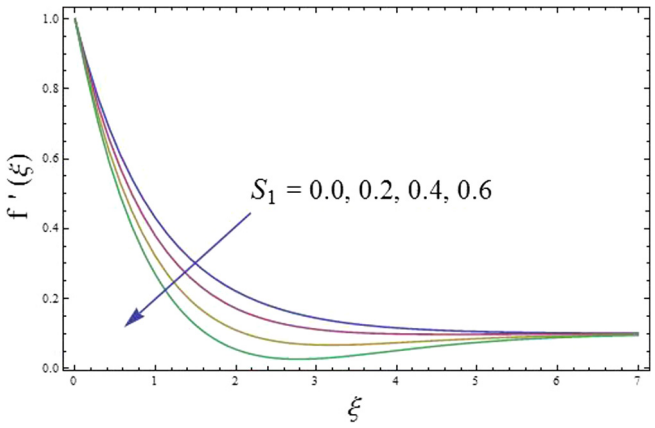

Fig. 6. Effect of thermal stratified parameter S_1 on axial velocity $f'(\xi)$.

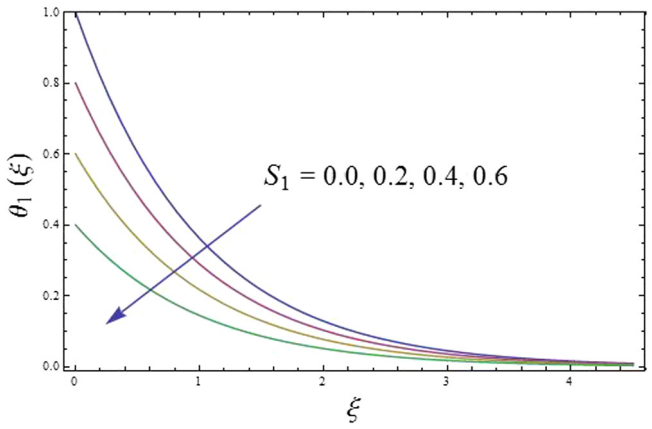

Fig. 7. Influence of thermal stratified parameter S_1 on temperature profile $\theta_1(\xi)$.

illustrates the enhancement in temperature and increases the thermal boundary layer thickness.

The effect of parameter Pr *(Prandtl number)*

The Pr (Prandtl number) is the silent characteristic number for thermal boundary layers and heat transfer in forced convection. The Pr (Prandtl number) is a measure of the ratio of heat transmission and energy storage capacities of the molecules. Fig. 10 exhibits the influence of parameter Pr (Prandtl number) on temperature field. It is designated that due to increasing parameter Pr, thermal diffusivity decreases. As a result, the temperature and thermal boundary layer thickness decrease. Fig. 11 indicates the enhancement in axial velocity for higher values of parameter Pr (Prandtl number).

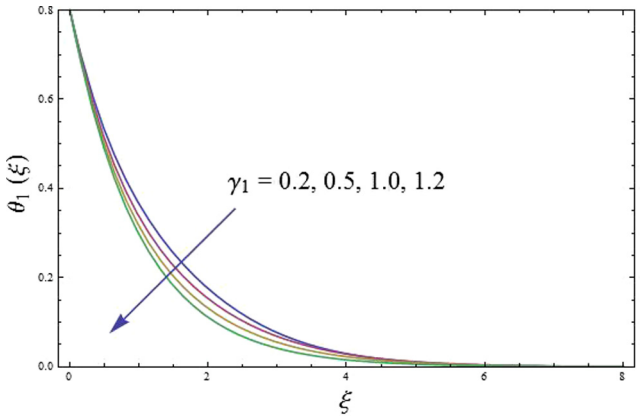

Fig. 8. Influence of parameter γ_1 (Deborah number) on temperature distribution $\theta_1(\xi)$.

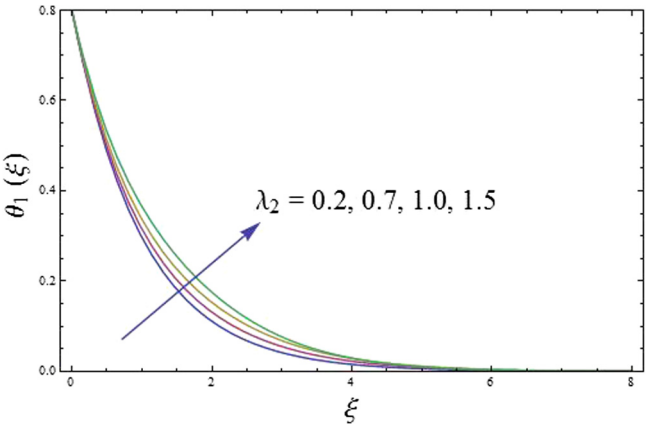

Fig. 9. Effect of ratio of relaxation to retardation time λ_2 on temperature distribution $\theta_1(\xi)$.

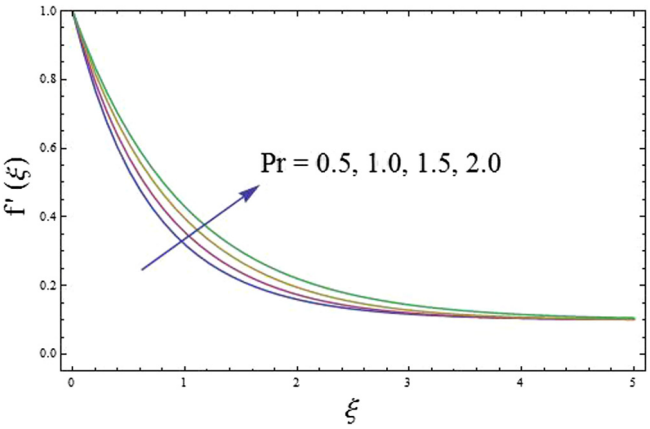

Fig. 10. Impact of Prandtl number Pr on axial velocity $f'(\xi)$.

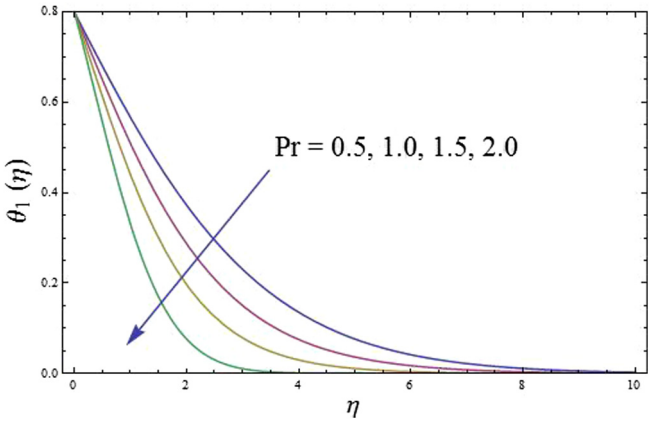

Fig. 11. Effect of Prandtl number Pr on temperature field $\theta_1(\xi)$.

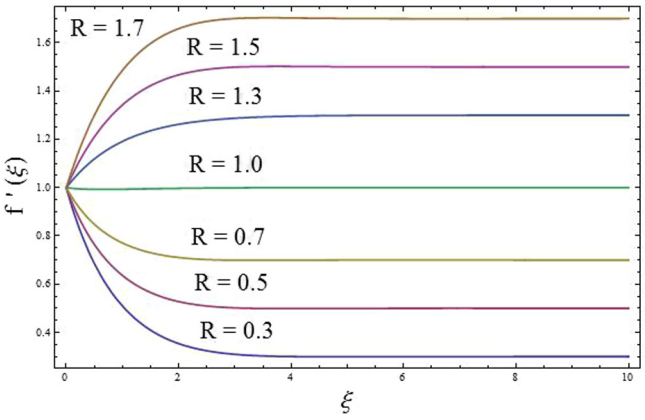

Fig. 12. Influence of ratio parameter R on velocity distribution $f'(\xi)$.

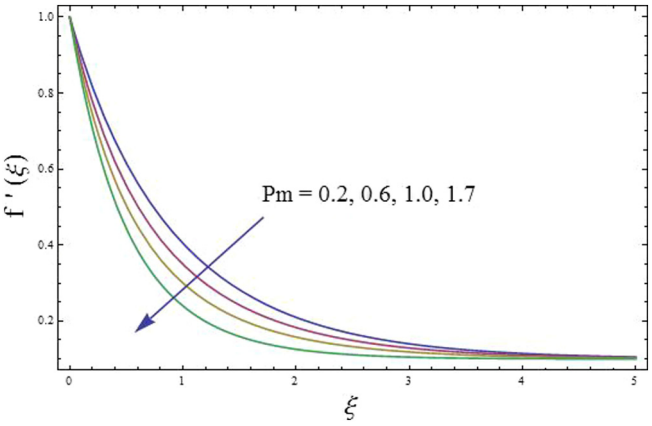

Fig. 13. Effect of porosity parameter P_m on velocity distribution $f'(\xi)$.

The effect of parameters R (ratio) and P_m (porosity)

The stretchable sheet causes the change in velocities of the fluid and a parameter R is introduced, which is the ratio of ambient fluid velocity to surface velocity. The parameter R has a peculiar behavior on axial velocity observed in Fig. 12. The parameter R have contrasting behavior for $R > 1$ and for $R < 1$. Moreover, axial velocity remains constant for $R = 1.0$. Axial velocity is rising by the increment in ratio parameter R. Whereas Fig. 13 display the impact of porosity parameter P_m on velocity. It is perceived that for increasing values of porosity parameter, axial velocity increases.

Skin friction coefficient and local Nusselt number

Impact of various parameters R, S_1 and Pr are observed on skin friction coefficient and Nusselt number. The enhancement in parameter R causes an increase in skin friction coefficient. More-

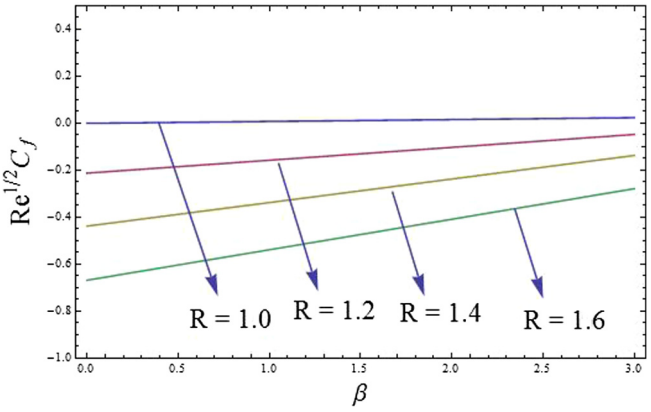

Fig. 14. Wall shear stress versus R.

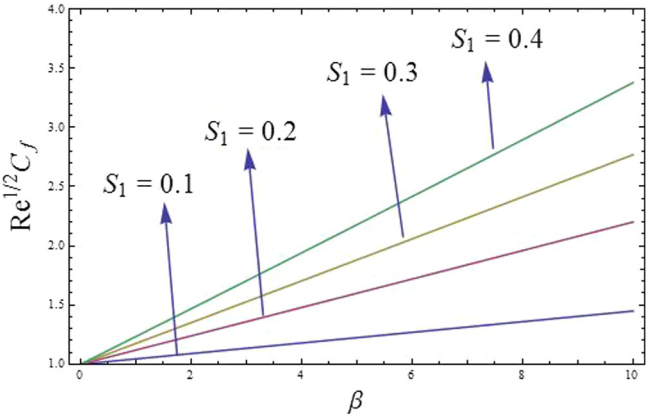

Fig. 15. Wall shear stress versus S_1.

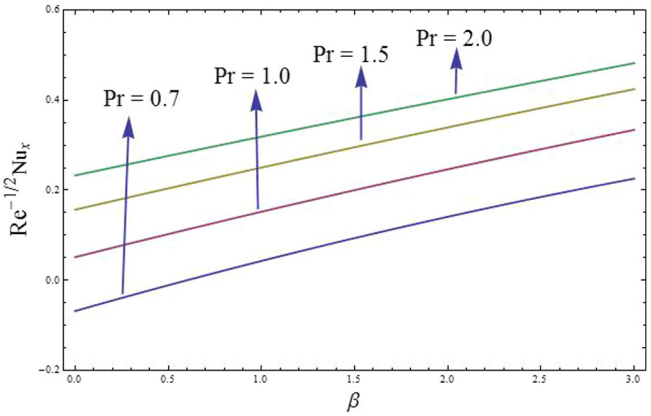

Fig. 16. Heat transfer rate versus Pr.

over, skin friction coefficient declines because plate velocity is hindered by fluid velocity for greater values of parameter R causing an increase in axial velocity. The fluid velocity and sheet velocity are same due to stretching at $R = 0$, causing no change in the graph Fig. 14. Further, the ascending behavior of stratification parameter S_1 enhances the wall shear stress observed in Fig. 15. In addition, heat transfer rate reduces due to variation in parameter Pr (Prandtl number) but the increment of S_1 (thermal stratification) results in an increase of heat transfer rate shown in Figs. 16 and 17, respectively.

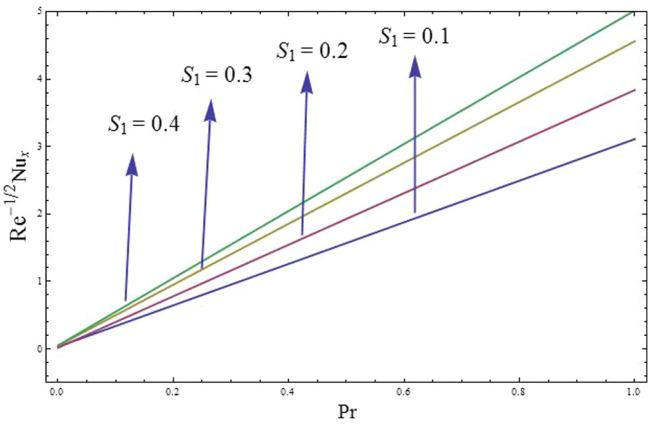

Fig. 17. Heat transfer rate versus S_1.

Concluding remarks

The aspects of thermal stratification on the ferrofluid past a horizontally stretchable surface under the influence of Magnetic dipole is under discussion. Bvph2 and Optimal HAM are used to get the numerical and analytic series solution for flow problem. The consequences of a few physical parameters, for example, ferromagnetic interaction parameter β, ratio of relaxation to retardation times λ_2, thermally stratified parameter S_1, Deborah number γ_1, ratio parameter R, Prandtl number Pr and porosity parameter Pm on velocity and temperature fields are inspected and discussed graphically in points of interest. At last, Some critical perceptions in view of the present study are as per the following.

An increase in parameter β (ferromagnetic interaction) gives rise to heat transfer thereby reducing axial velocity.

- Higher values of parameter S_1 (thermal stratification) corresponds to thinning of velocity and temperature fields. Further, the heat transfer rate enhances for increasing values of parameter S_1.
- Variation in parameter R (ratio) results in an increment in axial velocity, while the wall shears stress decreases.
- Axial velocity increases as we enhance the porosity parameter Pm.
- Prandtl number results in depletion in the temperature field while enhancement in axial velocity.

References

[1] Stephen PS. Low viscosity magnetic fluid obtained by the colloidal suspension of magnetic particles. Harvard; 1965.
[2] Mee CD. The mechanism of colloid agglomeration in the formation of bitter patterns. Proc Phys Soc 1950;8:922.
[3] Andersson HI, Valnes OA. Flow of a heated ferrofluid over a stretching sheet in the presence of a magnetic dipole. Acta Mech 1998;128:39–47.
[4] Neuringer JL. Some viscous flows of a saturated ferro-fluid under the combined influence of thermal and magnetic field gradients. Int J Non Linear Mech 1966;1:123–37.
[5] Tzirtzilakis EE, Kafoussias NG, Raptis A. Numerical study of forced and free convective boundary layer flow of a magnetic fluid over a flat plate under the action of a localized magnetic field. ZAMP 2010;61:929–47.
[6] Sharma D, Sharma RC. Effect of dust particles on thermal convection in ferromagnetic fluid saturating a porous medium. J Magn Magn Mater 2005;288:183–95.
[7] Majeed A, Zeeshan A, Ellahi R. Unsteady ferromagnetic liquid flow and heat transfer analysis over a stretching sheet with the effect of dipole and prescribed heat flux. J Mol Liq 2016;223:528–33.
[8] Sharma A, Sharma D, Sharma RC. Effect of dust particles on thermal convection in a ferromagnetic fluid. Z Naturforsch A 2005;60:494–502.
[9] Mee CD. The mechanism of colloid agglomeration in the formation of bitter patterns. Proc Phys Soc Sect A 1950;8:922.

[10] Eringen AC, Maugin GA. Electrodynamics of continua II, fluids and complex media. New York: Springer; 1990.
[11] Albrecht T, Bührer C, Fähnle M, Maier K, Platzek D, Reske J. First observation of ferromagnetism and ferromagnetic domains in a liquid metal. Appl Phys A 1997;2:215–20.
[12] Srinivasacharya D, Upendar M. Effect of double stratification on MHD free convection in a micropolar fluid. J Egypt Math Soc 2013;3:370–8.
[13] Foisal AA, Alam M. Unsteady free convection fluid flow over an inclined plate in the presence of a magnetic field with thermally stratified high porosity medium. J Appl Fluid Mech 2016;9.
[14] Antoniadis PD, Papalexandris MV. Numerical study of unsteady, thermally-stratified shear flows in superposed porous and pure-fluid domains. Int J Heat Mass Transfer 2016;96:643–59.
[15] Ganesh NV, Hakeem AKA, Ganga B. Darcy–Forchheimer flow of hydromagnetic nanofluid over a stretching/shrinking sheet in a thermally stratified porous medium with second order slip, viscous and Ohmic dissipations effects. Ain Shams Eng J 2016.
[16] Ferdows M, Liu D. The effect of inertia on free convection from a horizontal surface embedded in a porous medium, with internal heat generation. J Phys Math 2016.
[17] Nadeem S, Mehmood R, Akbar NS. Combined effects of magnetic field and partial slip on obliquely striking rheological fluid over a stretching surface. J Magn Magn Mater 2015;378:457–62.
[18] Rashidi S, Dehghan M, Ellahi R, Riaz M, Abad MTJ. Study of stream wise transverse magnetic fluid flow with heat transfer around an obstacle embedded in a porous medium. J Magn Magn Mater 2015;378:128–37.
[19] Akbar NS, Khan ZH. Magnetic field analysis in a suspension of gyrotactic microorganisms and nanoparticles over a stretching surface. J Magn Magn Mater 2016;410:72–80.
[20] Nadeem S, Muhammad N. Impact of stratification and Cattaneo-Christov heat flux in the flow saturated with porous medium. J Mol Liq 2016;224:423–30.
[21] Nadeem S, Haq RU, Akbar NS. MHD three-dimensional boundary layer flow of casson nanofluid past a linearly stretching sheet with convective boundary condition. IEEE Trans Nanotechnol 2014;1:109–15.
[22] Akbar NS, Tripathi D, Khan ZH, Bég OA. A numerical study of magnetohydrodynamic transport of nanofluids over a vertical stretching sheet with exponential temperature-dependent viscosity and buoyancy effects. Chem Phys Lett 2016;661:20–30.
[23] Akbar NS, Khan ZH. Effect of variable thermal conductivity and thermal radiation with CNTS suspended nanofluid over a stretching sheet with convective slip boundary conditions: numerical study. J Mol Liq 2016;222:279–86.
[24] Akbar NS, Khan ZH. Variable fluid properties analysis with water based CNT nanofluid over a sensor sheet: numerical solution. J Mol Liq 2017;232:471–7.
[25] Nayak MK, Akbar NS, Pandey VS, Khan ZH, Tripathi D. 3D free convective MHD flow of nanofluid over permeable linear stretching sheet with thermal radiation. Powder Technol 2017;315:205–15.
[26] Shirvan KM, Mamourian M, Mirzakhanlari S, Ellahi R, Vafai K. Numerical investigation and sensitivity analysis of effective parameters on combined heat transfer performance in a porous solar cavity receiver by response surface methodology. Int J Heat Mass Transfer 2017;105:811–25.
[27] Ellahi R, Tariq MH, Hassan M, Vafai K. On boundary layer nano-ferroliquid flow under the influence of low oscillating stretchable rotating disk. J Mol Liq 2017;229:339–45.
[28] Majeed A, Zeeshan A, Ellahi R. Unsteady ferromagnetic liquid flow and heat transfer analysis over a stretching sheet with the effect of dipole and prescribed heat flux. J Mol Liq 2016;223:528–33.
[29] Ellahi R, Tariq MH, Hassan M, Vafai K. On boundary layer nano-ferroliquid flow under the influence of low oscillating stretchable rotating disk. J Mol Liq 2017;229:339–45.
[30] Zeeshan A, Majeed A, Ellahi R. Effect of magnetic dipole on viscous ferro-fluid past a stretching surface with thermal radiation. J Mol Liq 2016;215:549–54.
[31] Shirvan KM, Ellahi R, Mirzakhanlari S, Mamourian M. Enhancement of heat transfer and heat exchanger effectiveness in a double pipe heat exchanger filled with porous media: numerical simulation and sensitivity analysis of turbulent fluid flow. Appl Therm Eng 2016;109:761–74.
[32] Muhammad N, Nadeem S, Haq RU. Heat transport phenomenon in the ferromagnetic fluid over a stretching sheet with thermal stratification. Results Phys 2017;7:854–61.
[33] Muhammad N, Nadeem S, Mustafa T. Squeezed flow of a nanofluid with Cattaneo-Christov heat and mass fluxes. Results Phys 2017;7:862–9.
[34] Nadeem S, Ahmad S, Muhammad N. Cattaneo-Christov flux in the flow of a viscoelastic fluid in presence of Newtonian heating. J Mol Liq 2017.
[35] Salahuddin T, Khan I, Malik MY, Khan M, Hussain A, Awais M. Internal friction between fluid particles of MHD tangent hyperbolic fluid with heat generation: using coefficients improved by Cash and Karp. Eur Phys J Plus 2017;132:1–10.
[36] Liao SJ. Beyond perturbation: introduction to homotopy analysis method. Boca Raton: Chapman and Hall, CRC Press; 2003.
[37] Liao SJ. Homotopy analysis method in non-linear differential equations. Heidelberg: Springer and Higher Education Press; 2012.
[38] Abel MS, Sanjayanand E, Nandeppanavar MM. Viscoelastic MHD flow and heat transfer over a stretching sheet with viscous and ohmic dissipations. Commun Nonlinear Sci Numer Simul 2008;13:1808–21.